

See discussions, stats, and author profiles for this publication at: <https://www.researchgate.net/publication/324604162>

# Enzyme-Regulated DNA-Based Logic Device

Article in ACS Synthetic Biology · April 2018

DOI: 10.1021/acssynbio.8b00088

CITATIONS

12

READS

153

4 authors:



**Manish Debnath**

Indian Institute of Chemical Biology

18 PUBLICATIONS 449 CITATIONS

SEE PROFILE



**Rakesh Paul**

Indian Association for the Cultivation of Science

10 PUBLICATIONS 192 CITATIONS

SEE PROFILE



**Deepanjan Panda**

Indian Association for the Cultivation of Science

15 PUBLICATIONS 275 CITATIONS

SEE PROFILE



**Jyotirmayee Dash**

Indian Association for the Cultivation of Science

142 PUBLICATIONS 3,156 CITATIONS

SEE PROFILE

Some of the authors of this publication are also working on these related projects:



G-quadruplex, Logic devices [View project](#)



Targeting DNA secondary structures for cancer therapeutics [View project](#)

## Enzyme-Regulated DNA-Based Logic Device

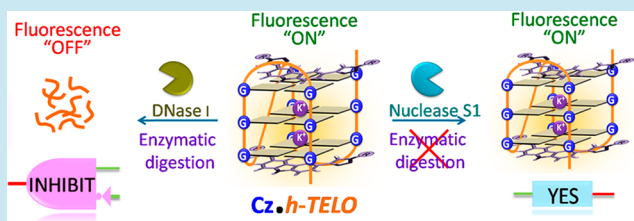
Manish Debnath, Rakesh Paul, Deepanjan Panda, and Jyotirmayee Dash\*<sup>1</sup>

Department of Organic Chemistry, Indian Association for the Cultivation of Science, Kolkata 700032, India

## Supporting Information

**ABSTRACT:** Herein, we report a carbazole (Cz) ligand that displays distinct turn-on fluorescence signals upon interaction with human telomeric G-quadruplex (*h-TELO*) and nuclease enzymes. Interestingly, Cz selectively binds and stabilizes the mixed hybrid topology of *h-TELO* G-quadruplex that withstands digestion by exonucleases and nuclease S1. The distinct fluorescence signatures of Cz-stabilized *h-TELO* with nucleases are used to design conceptually novel DNA devices for selectively detecting the enzymatic activity of DNase I as well as performing logic operations. An INHIBIT logic gate is constructed using *h-TELO* and DNase I as the inputs while the inputs of *h-TELO* and nuclease S1 form a YES logic gate. Furthermore, a two-input two-output reusable logic device with “multiset” function is developed by using *h-TELO* and DNase I as inputs. On the basis of this platform, combinatorial logic systems (INHIBIT–INHIBIT and NOR–OR) have been successfully installed using different combinations of nucleases as inputs. Moreover, this new strategy of using a synthetic dual emissive probe and enzyme/DNA inputs for constructing reusable logic device may find important applications in biological computing and information processing.

**KEYWORDS:** biomolecular device, DNA computation, dual emissive, G-quadruplex, nucleases



Nucleases play crucial roles in key biological processes like DNA replication, recombination and repair as they catalyze the cleavage of DNA phosphodiester bonds.<sup>1,2</sup> They are also considered as biomarkers for cancer and several other diseases.<sup>3,4</sup> Therefore, the development of new and sensitive devices that detect and distinguish enzymatic activity of nucleases would be useful in molecular biology and medical diagnosis applications.<sup>5</sup> DNA based probes have been developed to assess the activity of nucleases.<sup>6–11</sup> In recent years, DNA has been widely used as a versatile material for chemical and biological sensing and biomolecular computations due to their predictable structures, easy chemical synthesis and reactivity toward enzymes.<sup>12–29</sup> DNA structures (e.g., aptamers, DNAzymes, hydrogels *etc.*) that exhibit stimuli responsive behavior have been reported as components of computational systems.<sup>12–31</sup> However, the requirement of expensive fluorescent labeling and instrumentation techniques hinders the practical applications of DNA computation devices. In this work, we demonstrate a novel design platform comprising a dual emissive fluorescent probe<sup>32–36</sup> that simultaneously detects human telomeric DNA G-quadruplex (*h-TELO*) and nuclease enzymes (nuclease S1,<sup>37</sup> DNase I, T7 Endonuclease I, Exonucleases I and III) for constructing DNA devices.

DNA G-quadruplexes are four-stranded DNA secondary structures present in human telomeres and oncogene promoter regions. The G-quadruplexes are highly polymorphic structures; for instance, the *h-TELO* G-quadruplex can adopt mixed hybrid and antiparallel topologies in the presence of K<sup>+</sup> and Na<sup>+</sup> ions, respectively.<sup>38–42</sup> G-quadruplexes play key role in telomere maintenance and oncogene regulation and thus emerging as important biological targets for anticancer therapeutics.<sup>43–46</sup>

Small molecule fluorescent probes have been designed to selectively target DNA G-quadruplexes in biological system.<sup>38–42,47</sup> And further, G-quadruplex binding fluorescent probes have also been used for designing programmable logic devices.<sup>48–58</sup> We herein present a carbazole derivative (Cz)<sup>59,60</sup> (Figure 1, Scheme S1, Supporting Information, SI) that exhibits distinguishable turn-on fluorescence signatures for nucleases and G-quadruplexes. This carbazole probe exhibits salient

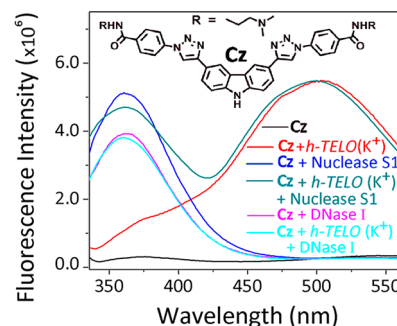


**Figure 1.** Structure of carbazole derivative (Cz) and fluorescence emission spectra of the Cz (1  $\mu$ M) in the presence and absence of 1  $\mu$ M *h-TELO* (K<sup>+</sup>) in 10 mM Tris-HCl, 100 mM KCl buffer (pH 7.4); 1  $\mu$ M nuclease S1 in 50% glycerol, 20 mM Tris-HCl, 30 mM KCl, 0.5 mM EDTA, 1 mM DTT buffer (pH 7.4); and 1  $\mu$ M DNase I in 10 mM Tris-HCl, 100 mM KCl, 2.5 mM MgCl<sub>2</sub>, 0.1 mM CaCl<sub>2</sub> buffer (pH 7.4).

Received: February 26, 2018

features: (i) high selectivity for the mixed hybrid-type conformation of *h*-TELO G-quadruplex, (ii) ability to switch the antiparallel conformation of *h*-TELO to mixed hybrid type quadruplex, (iii) protection of *h*-TELO against digestion by exonucleases and nuclease S1 and (iv) serving as a reporter for the detection of DNase I enzymatic activity. Importantly, the differential fluorescence behavior of **Cz**-stabilized *h*-TELO in the presence of different nucleases is used to construct various logic devices for biocomputation and diagnostics.

## RESULTS AND DISCUSSION

The interaction of **Cz** with quadruplexes was evaluated using fluorescence spectroscopy, melting analysis by Förster resonance energy transfer (FRET)<sup>61</sup> and circular dichroism (CD) spectroscopy. We have used a 24-mer *h*-TELO sequence that folds into mixed hybrid-type quadruplex structure in K<sup>+</sup> buffer, i.e., *h*-TELO (K<sup>+</sup>) and antiparallel G-quadruplex in Na<sup>+</sup> buffer, i.e., *h*-TELO (Na<sup>+</sup>). The *h*-TELO sequence was also annealed in MQ water (pH 7.4) (in the absence of salt) and used as free *h*-TELO. In addition, we have used three parallel-type oncogenic promoter G-quadruplexes like *c*-MYC, *c*-KIT1 and *c*-KIT2 and a control duplex (*ds*) DNA.

**Cz Preferentially Interacts with Mixed Hybrid-Type *h*-TELO G-Quadruplex.** Carbazole derivative **Cz** showed two weak emission peaks at 373 and 530 nm (quantum yield,  $\phi = 0.019$  and 0.016, respectively,  $\lambda_{\text{ex}} = 320$  nm) in 100 mM KCl, 10 mM Tris-HCl at pH 7.4 (Figure S1 and S2A, SI). Upon addition of DNA quadruplexes (1  $\mu\text{M}$ ), the fluorescence intensity of **Cz** was enhanced at 530 nm but no significant changes were detected at 373 nm (Figure S2, SI). **Cz** (1  $\mu\text{M}$ ) exhibited a strong (14-fold) turn-on fluorescence signal at 530 nm with a 40 nm blue shift in the presence of 1  $\mu\text{M}$  *h*-TELO (K<sup>+</sup>); while only a 5 fold increase at 530 nm along with a 25 nm blue shift was observed in the presence of 1  $\mu\text{M}$  *h*-TELO (Na<sup>+</sup>) (Figure 2A and Table 1). Interestingly, the fluorescence intensity of **Cz** was increased 6 fold (26 nm blue shift) in the

**Table 1.** The  $K_d$ ,  $F/F_0$  (at 1  $\mu\text{M}$ ) and Concentration of **Cz** at  $\Delta T_m^{\text{max}}$  with Different Quadruplexes Used in This Study

DNA sequences	$K_d^a$	$F/F_0$ (1 $\mu\text{M}$ )	[ <b>Cz</b> ] at $\Delta T_m^{\text{max}}$ <sup>b</sup>
<i>h</i> -TELO (K <sup>+</sup> ): 5'- d(T <sub>2</sub> G <sub>3</sub> T <sub>2</sub> AG <sub>3</sub> T <sub>2</sub> AG <sub>3</sub> T <sub>2</sub> AG <sub>3</sub> A)-3'	0.15	14	100 nM
<i>h</i> -TELO (Na <sup>+</sup> ): 5'- d(T <sub>2</sub> G <sub>3</sub> T <sub>2</sub> AG <sub>3</sub> T <sub>2</sub> AG <sub>3</sub> T <sub>2</sub> AG <sub>3</sub> A)-3'	0.9	5	600 nM
<i>h</i> -TELO (free): 5'- d(T <sub>2</sub> G <sub>3</sub> T <sub>2</sub> AG <sub>3</sub> T <sub>2</sub> AG <sub>3</sub> T <sub>2</sub> AG <sub>3</sub> A)-3'	0.6	6	600 nM
<i>c</i> -MYC: 5'-d(TGAG <sub>3</sub> TG <sub>3</sub> TAG <sub>3</sub> TG <sub>3</sub> TA <sub>2</sub> )- 3'	0.45	6	200 nM
<i>c</i> -KIT1: 5'-d(G <sub>3</sub> AG <sub>3</sub> CGCTG <sub>3</sub> AG <sub>3</sub> AG <sub>3</sub> )-3'	1.7	3	800 nM
<i>c</i> -KIT2: 5'-d(G <sub>3</sub> CG <sub>3</sub> CGCGAG <sub>3</sub> AG <sub>4</sub> )-3'	1.9	3	1000 nM
<i>ds</i> DNA: <sup>c</sup> 5'-d(TATAGCTATA HEG TATAGCTATA)-3'	N.D.	—	—

<sup>a</sup> $K_d$  in  $\mu\text{M}$  (Error =  $\pm 5\%$ ), determined from Hill equation. <sup>b</sup> $\Delta T_m^{\text{max}}$  =  $\Delta T_m$  value to attain a maximum  $T_m$  of 93 °C. <sup>c</sup>HEG = Hexaethylene glycol.

presence of 1  $\mu\text{M}$  free *h*-TELO, suggesting that **Cz** could fold the free *h*-TELO into a G-quadruplex structure. Similarly, **Cz** exhibited 3–6 fold fluorescence enhancements and 24–26 nm blue shifts in the presence of 1  $\mu\text{M}$  parallel-type *c*-MYC, *c*-KIT1 and *c*-KIT2 quadruplexes. Fluorescence binding titration of **Cz** with G-quadruplex and *ds* DNA targets showed that **Cz** interacted with *h*-TELO (K<sup>+</sup>) with considerably high affinity with a dissociation constant ( $K_d$ ) of 150 nM compared to the *h*-TELO (Na<sup>+</sup>) ( $K_d = 900$  nM), free *h*-TELO ( $K_d = 600$  nM) and promoter quadruplexes like *c*-MYC ( $K_d = 450$  nM), *c*-KIT1 ( $K_d = 1.7$   $\mu\text{M}$ ) and *c*-KIT2 ( $K_d = 1.9$   $\mu\text{M}$ ) (Figure 2B and S3, Table S1, SI). Importantly, *ds* DNA did not influence the emission peaks of **Cz**, indicating its negligible binding affinity toward *ds* DNA.

The binding stoichiometry of **Cz** with quadruplexes was determined by monitoring the change in fluorescence intensity as a function of the mole fraction of ligand (Job's plot). The Job's plot analysis revealed that **Cz** binds to *h*-TELO with a 2:1 stoichiometry, while a 1:1 stoichiometry was observed with parallel quadruplexes (Figure S4, Table S1, SI). Molecular modeling analysis further supported that **Cz** could stack on both terminals of the *h*-TELO mixed hybrid-type quadruplex (Figure S5, SI).

The FRET melting analysis revealed that **Cz** showed a maximum stabilization potential for *h*-TELO (K<sup>+</sup>) with a  $\Delta T_m$  value of 36 °C ( $T_m$  of 93 °C) at 100 nM; whereas, higher concentrations of **Cz** (600 nM) were required to achieve saturation in  $\Delta T_m$  values for free *h*-TELO and *h*-TELO (Na<sup>+</sup>) (Figure S6, Table S1, SI). Similarly, 2–10 fold higher concentrations of **Cz** were required to attain maximum  $\Delta T_m$  values for parallel G-quadruplexes; 200 nM for *c*-MYC ( $\Delta T_m = 24$  °C,  $T_m = 93$  °C), 800 nM for *c*-KIT1 ( $\Delta T_m = 39$  °C,  $T_m = 93$  °C) and 1  $\mu\text{M}$  for *c*-KIT2 ( $\Delta T_m = 29$  °C,  $T_m = 93$  °C). These results are in agreement with fluorescence binding titrations, suggesting **Cz** selectively recognizes and stabilizes the *h*-TELO mixed hybrid-type quadruplex structure over parallel, antiparallel type quadruplexes and *ds* DNA.

**Cz Induces a Conformational Switch.** To further ascertain the selectivity of **Cz** for the mixed hybrid topology, CD spectroscopic analysis of *h*-TELO quadruplex was performed in the presence and absence of metal ions (Na<sup>+</sup> and K<sup>+</sup>). The CD spectrum of *h*-TELO (K<sup>+</sup>) exhibited a positive peak at 290 nm and a shoulder at 260 nm, characteristic of a mixture of parallel and antiparallel

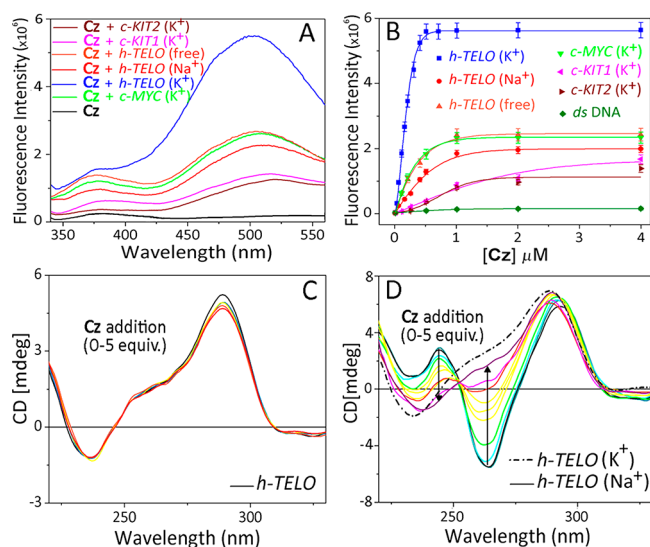


**Figure 2.** (A) Fluorescence emission of **Cz** (1  $\mu\text{M}$ ) in the presence of different DNA quadruplexes (1  $\mu\text{M}$ ); (B) Fluorescence titration of **Cz** (1  $\mu\text{M}$ ) with different G-quadruplexes and *ds* DNA (0–4  $\mu\text{M}$ ). CD spectra of 5  $\mu\text{M}$  (C) *h*-TELO (K<sup>+</sup>) in 10 mM Tris-HCl 100 mM KCl buffer (pH 7.4); and (D) *h*-TELO (Na<sup>+</sup>) upon addition of **Cz** (0–5 equiv) in 10 mM Tris-HCl 100 mM NaCl buffer (pH 7.4).

conformations (Figure 2C and S7A, SI). No further changes in the peaks were observed after titration with 0–5 equiv Cz, indicating that ligand does not alter the mixed hybrid topology of *h*-TELO G-quadruplex.

The *h*-TELO (Na<sup>+</sup>) showed a positive peak at 290 nm, a negative peak at 260 nm and a positive peak at 245 nm, characteristic of an antiparallel topology (Figure 2D). Interestingly, when *h*-TELO (Na<sup>+</sup>) was titrated with 0–5 equiv Cz, the negative peak at 260 nm was gradually diminished and a new positive shoulder at 260 nm was developed. In addition, the positive peak at 245 nm was completely disappeared whereas the positive peak, at 290 nm remained almost unchanged. This suggests that Cz-stabilized *h*-TELO structure is similar in both K<sup>+</sup> and Na<sup>+</sup> buffers.

It is worth noting that Cz could induce the formation of a mixed hybrid conformation of the *h*-TELO quadruplex even in the absence of any metal ions (Figure S7B and Scheme S2, SI). As shown in Figure S7B, the free *h*-TELO, in the presence of Cz in MQ water (pH 7.4), showed a similar spectral pattern as in K<sup>+</sup> buffer. No significant changes in the CD spectra were observed upon titrations of parallel quadruplexes (*c*-MYC, *c*-KIT1 and *c*-KIT2) with Cz (Figure S8, SI), suggesting the preference of Cz to induce a mixed hybrid quadruplex topology.

**Cz Binds to Nucleases and Exhibits Distinct Fluorescence Signal.** We observed that Cz could interact with nuclease S1 and DNase I, and exhibited a distinct fluorescence signature compared to quadruplexes (Figure 1 and S9, SI). Upon treatment with nucleases, Cz showed strong fluorescence turn-on signals at 373 nm whereas fluorescence turn-on responses at 530 nm were noted in the presence of quadruplexes. Control studies showed that the nucleases do not exhibit any significant turn-on emission upon excitation at 320 nm in the absence of Cz (Figure S10, SI). From the fluorescence binding studies, the  $K_d$  values for nuclease S1 and DNase I were determined to be 1.3  $\mu$ M and 2.5  $\mu$ M, respectively (Table S2, SI). In order to understand the binding sites of Cz on nucleases, a reverse titration was carried out by incremental addition of Cz to the nucleases (Figure S11, SI). Enzymes show a peak at 330 nm due to the presence of aromatic amino acid residues. The emission of nucleases at 330 nm was monitored by exciting at 280 nm. Notably, upon addition of Cz, the emission peaks of the nucleases were shifted to longer wavelengths ( $\sim$ 37 nm red shift) with a concomitant decrease in fluorescence intensity (Figure S11, SI). This decrease in fluorescence intensity may be due to the energy transfer resulting from partial overlap between the emission spectra of enzymes and absorption spectra of Cz. The red-shifted emission and fluorescence quenching indicate that Cz binds to the aromatic residues present in the nucleases. The Job's plot analysis revealed that Cz binds to nucleases with a 1:1 stoichiometry (Figure S12, SI). CD spectroscopic analysis suggested that Cz does not alter the conformation of nuclease S1 and DNase I (Figure S13, SI).

In order to gain insight into the different fluorescence spectral behavior of Cz with nucleases and quadruplexes, the microenvironments of the Cz were investigated in solvents of different polarity (Figure S14A, SI). Cz, which is weakly fluorescent in aqueous media shows significant increase in emission intensity in hydrophobic environments (Figure S14B, SI). It was observed that by decreasing the solvent polarity, the fluorescence emission maxima ( $\lambda_{\text{max}}^{\text{em}}$ ) of Cz was blue-shifted and the Stokes shift (S) values of Cz were decreased (Table S3,

SI). These observations suggest that the enhancement in the fluorescence intensity along with the blue shift in the  $\lambda_{\text{max}}^{\text{em}}$  of the Cz is a consequence of the changing microenvironments of Cz upon binding with quadruplexes and nucleases. The dual emissive nature of Cz may be due to the locally excited state and intramolecular charge transfer, which is promoted by the extended conjugation along with electron donating amino and acceptor carbonyl groups.<sup>62–64</sup>

The  $\lambda_{\text{max}}^{\text{em}}$  of Cz in different solvents were plotted against Reichardt's  $E_T(30)$  polarity parameter (Figure S14C, SI). A linear dependence of  $\lambda_{\text{max}}^{\text{em}}$  ( $y = 4.9x + 217.9$ ,  $r^2 = 0.9735$ ) on the polarity, i.e.,  $E_T(30)$  of the solvent media was noted. The  $E_T(30)$  values obtained for Cz in the presence of *h*-TELO G-quadruplex and nucleases were determined to be 56.1 and 30.5. These results indicate a close proximity of Cz to the hydrophobic binding domain of the *h*-TELO G-quadruplex and corroborate with the molecular docking studies that showed end-stacking mode of Cz to the external G-quartet of the quadruplex. The  $E_T(30)$  values further suggest that Cz binds to the nucleases in hydrophobic binding pocket, rich in aromatic amino acid residues. These results were in agreement with molecular docking analysis which indicated that Cz binds to nuclease S1 and DNase I in a site rich in aromatic amino acid residues (Figure S15, SI).

**Sensor Design and Detection of DNase I Activity.** As Cz showed distinct fluorescence turn-on responses for quadruplexes and nucleases, it was employed to monitor the activity of the nucleases on *h*-TELO in the presence and absence of K<sup>+</sup> ions (Figure 3A, 3B, 4A and S16, SI). Nuclease S1 readily cleaves the phosphate backbone of the DNA at single stranded region. However, upon addition of nuclease S1 to Cz-stabilized *h*-TELO quadruplex in K<sup>+</sup> buffer, the peak at 530 nm remained unaffected with the generation of a new peak at 373

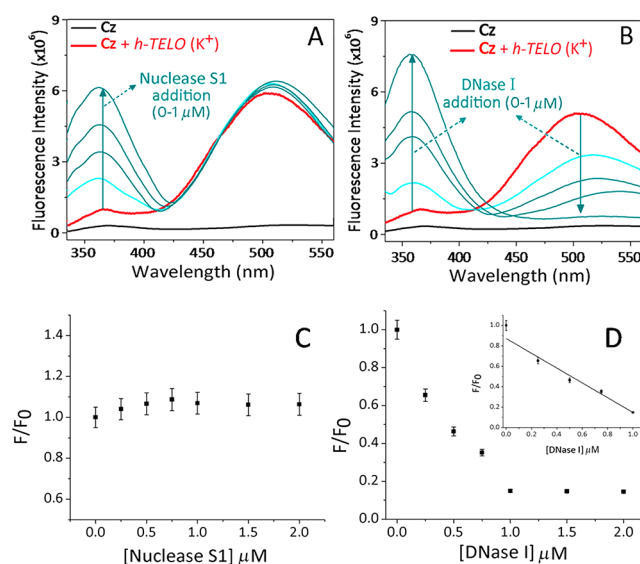


**Figure 3.** Emission spectra of (A) Cz (1  $\mu$ M) in the presence of *h*-TELO (K<sup>+</sup>) (1  $\mu$ M) (red) and upon titration with nuclease S1 (0–1  $\mu$ M) (cyan); (B) Cz (1  $\mu$ M) in the presence of *h*-TELO (K<sup>+</sup>) (1  $\mu$ M) (red) and upon titration with DNase I (0–1  $\mu$ M) (cyan). The change in fluorescence intensity ( $F/F_0$ ) of Cz-stabilized *h*-TELO (K<sup>+</sup>) at 530 nm (C) upon titrating with nuclease S1 (0–2  $\mu$ M); (D) upon titrating with DNase I (0–2  $\mu$ M) and the linear dependence of fluorescence intensity of Cz-stabilized *h*-TELO (K<sup>+</sup>) with increasing DNase I (0–1  $\mu$ M) (inset).

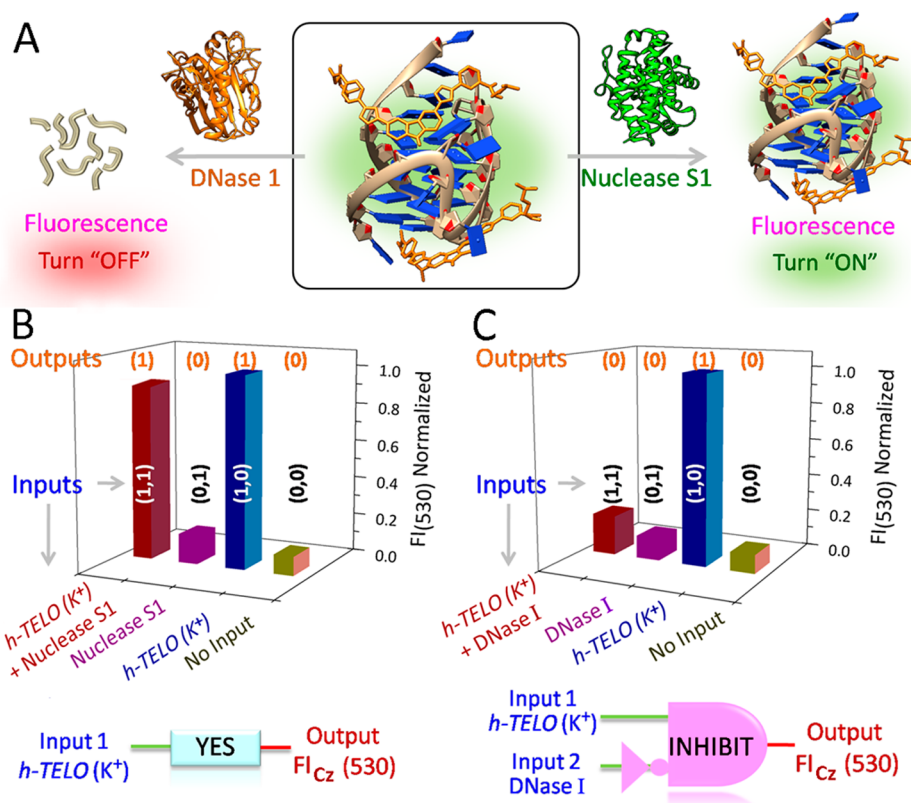


**Figure 4.** (A) Schematic representation of the distinct spectral behavior of Cz with *h*-TELO ( $K^+$ ) (PDB ID: 2JPZ) and nucleases. Logic behavior of Cz (B) when  $1 \mu\text{M}$  of *h*-TELO ( $K^+$ ) and nuclease S1 are inputs; (C) when  $1 \mu\text{M}$  of *h*-TELO ( $K^+$ ) and DNase I are inputs.

nm. Similar spectra were obtained when nuclease S1 was added to Cz-stabilized *h*-TELO system in the absence of  $K^+$  ions. These results indicate that Cz is able to bind both *h*-TELO and nuclease S1 and further protects *h*-TELO against nuclease S1 enzymatic degradation by inducing and stabilizing G-quadruplex structure in the presence and absence of  $K^+$  ions (Figure 3A and S16C, SI).

To exclude the possibility of competitive displacement of Cz from *h*-TELO to nucleases, titration of Cz was carried out with a 1:1 mixture of *h*-TELO ( $K^+$ ) and nucleases in  $K^+$  buffer (Figure S16A and S16B, SI). A single peak was observed at 373 nm with the disappearance of 530 nm peak, which suggests that nuclease S1 is able to digest *h*-TELO in the absence of Cz induced stabilization. In addition, Cz exhibited no competitive enhancement in the emission peaks, thereby excluding the possibility of competitive binding. On the other hand, DNase I could digest Cz-stabilized *h*-TELO into small fragments in the presence and absence of metal ions. The formation of a new peak at 373 nm was observed upon addition of DNase I into Cz-stabilized *h*-TELO with the complete disappearance of the peak at 530 nm (Figure 3B and S16D, SI). These results were supported by CD spectroscopy as the characteristic CD peaks of Cz-stabilized *h*-TELO at 290 and 270 nm were preserved in the presence of nuclease S1 ( $2 \mu\text{M}$ ), however the peaks were gradually diminished upon titrating with 0– $1 \mu\text{M}$  of DNase I (Figure S17, SI).

To investigate the selectivity of the system, Cz-stabilized *h*-TELO was also titrated with Exo I (single strand specific exonuclease), Exo III (duplex specific exonuclease) and T7 Endonuclease I. Cz bound *h*-TELO exhibited distinct fluorescence response for exonucleases and T7 Endonuclease I (Figure S18, SI). Upon titration with T7 Endonuclease I (0– $4$

$\mu\text{M}$ ), the 530 nm peak of Cz-stabilized *h*-TELO was gradually decreased with a concomitant increase in 373 nm peak whereas Cz-stabilized *h*-TELO showed both peaks (373 and 530 nm) in the presence of exonucleases.

On the basis of the observations described above, the Cz-stabilized *h*-TELO was used to construct a sensor for detection of the DNase I enzymatic activity. As shown in Figure 3B, Cz exhibited high fluorescence intensity in the presence of  $1 \mu\text{M}$  *h*-TELO G-quadruplex in  $K^+$  buffer. Upon titration with 0 to  $2 \mu\text{M}$  DNase I, the fluorescent intensity of Cz-stabilized *h*-TELO was gradually decreased with saturation at  $1 \mu\text{M}$  DNase I concentration (Figure 3D). The inset in Figure 3D shows a linear relationship ( $R^2 = 0.973$ ) in the concentration range from 0 to  $1 \mu\text{M}$ . It was observed that the system could detect  $0.5 \mu\text{M}$  of DNase I (working concentration  $\sim 0.4$ – $35 \mu\text{M}$ ). And further, the system could selectively detect the enzymatic activity of DNase I over other nucleases used in the study (Figure S18D, SI). No significant change in the fluorescence intensity was observed upon titration of Cz-stabilized *h*-TELO with 0– $2 \mu\text{M}$  of nuclease S1, 0– $4 \mu\text{M}$  Exonuclease I (Exo I) and Exonuclease III (Exo III) (Figure S18, SI). It was found out that 4-fold higher concentration of T7 Endonuclease I ( $4 \mu\text{M}$ ) was required to digest Cz-stabilized *h*-TELO compared to DNase I. Therefore, the present DNase I sensing platform is selective, economical, sensitive and timesaving compared to the conventional methods.

**Enzyme-Regulated Logic Devices.** We envisioned that these distinct spectral behaviors of Cz with quadruplexes and nucleases could be used to construct logic devices to detect nuclease activity (Figure 4A). The *h*-TELO G-quadruplex and nucleases (nuclease S1 and DNase I) were used as inputs and the fluorescence intensity of the system at 530 nm was taken as

output. For output, >8 fold and <4 fold increase in fluorescence intensity of the system were defined as “1” and “0”, respectively. In the absence of any input (0,0), Cz showed a weak peak at 530 nm (output = 0) (Figure 4B). When *h*-TELO ( $K^+$ ) was used as the input (1,0), the fluorescence intensity at 530 nm increased sharply (output = 1). The input nuclease S1 (0,1) showed a negligible effect on the fluorescence of Cz at 530 nm, giving an output signal of “0”. In the presence of both the inputs (1,1), a strong signal at 530 nm (output = 1) was observed indicating that Cz binds to *h*-TELO ( $K^+$ ) with high affinity and inhibits nuclease S1 activity. The fluorescence responses of Cz in the presence and absence of inputs *h*-TELO ( $K^+$ ) and nuclease S1 were used to construct a Boolean logic gate, which is in accordance with a YES logic system.

On the contrary, when DNase I was used as one of the inputs, the fluorescence response of Cz in the presence of *h*-TELO was different (Figure 4C). By using *h*-TELO ( $K^+$ ) and DNase I as inputs (1,1), only a weak signal of Cz was observed at 530 nm (output = 0), due to the enzymatic degradation of *h*-TELO even in the presence of Cz. The truth table, using *h*-TELO ( $K^+$ ) and DNase I as the inputs, matches that for the INHIBIT logic system, where the gate (output) was activated only in the presence of *h*-TELO. It is important to note that similar logic gates could be constructed by using the free *h*-TELO as one of the inputs due to the ability of Cz to induce the formation of *h*-TELO G-quadruplex in the absence  $K^+$  ions (Figure S19, S20, Table S4, S5, S6 and S7, SI).

**Reusable Logic Devices with Multireset Function.** The degradation of Cz-stabilized *h*-TELO by DNase I enabled the construction of multireset reusable logic systems by using heat deactivation (HD) of DNase I after each cycle (Figure 5 and 6). The fluorescence signatures of Cz at 530 and 373 nm upon interaction with *h*-TELO and DNase I, respectively, were used as outputs.

In the presence of DNase I and *h*-TELO as the inputs (1,1), a weak signal at 530 nm (output<sub>530</sub> = 0) and an intense signal at 373 nm (output<sub>373</sub> = 1) were observed. By heating the mixture, the activity of DNase I was inhibited and the fluorescence

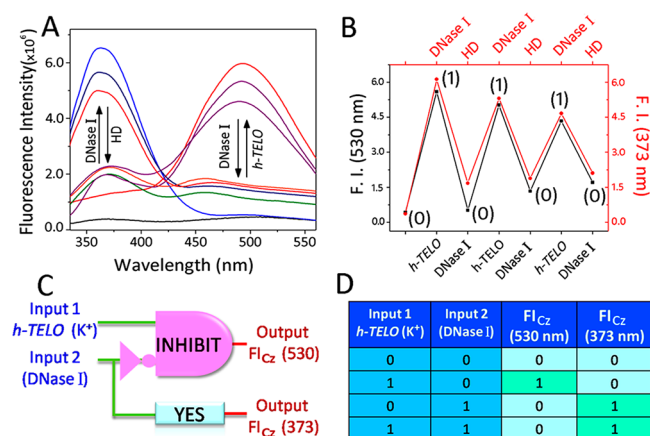


**Figure 5.** Reversible changes in (A) fluorescence spectra of Cz (1  $\mu$ M) (B) fluorescence intensity of Cz (1  $\mu$ M) at 530 and 373 nm in 10 mM Tris-HCl (pH 7.4), 100 mM KCl, 2.5 mM MgCl<sub>2</sub>, 0.1 mM CaCl<sub>2</sub> buffer upon sequential addition of 1  $\mu$ M of *h*-TELO ( $K^+$ ) and DNase I, followed by heat deactivation (HD) of DNase I; (C) Logic representation and (D) truth table for the system using *h*-TELO ( $K^+$ ) and DNase I as inputs and emission of Cz at 530 and 373 nm as outputs.

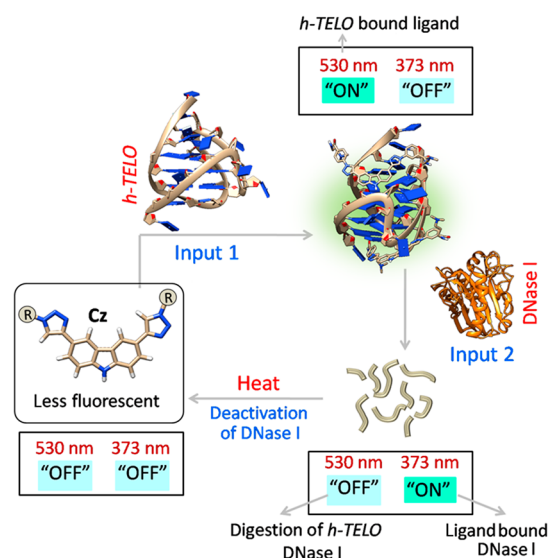


**Figure 6.** Schematic representation showing the multireset function of reusable logic device.

emission of Cz was restored with >80% efficiency. In the second cycle, when *h*-TELO (1,0) was added to the system, a significant increase in fluorescence intensity of Cz at 530 nm was observed (output<sub>530</sub> = 1). As expected, a strong emission at 373 nm (output<sub>373</sub> = 1) and a weak emission at 530 nm (output<sub>530</sub> = 0) were observed upon addition of DNase I (1,0). Therefore, an INHIBIT logic gate at output<sub>530</sub> and a YES logic gate at output<sub>373</sub> were constructed (Figure 5C and 5D) and these gates could be reusable by modulating the activity of DNase I. Three consecutive cycles using *h*-TELO ( $K^+$ )/DNase I/heat deactivation led only to a  $\sim$ 33% decrease in efficiency of the logic system. Therefore, the generated side products (digested *h*-TELO fragments and deactivated DNase I), showed limited effect on the logic system enabling efficient recycling.

**Enzyme Regulated Combinatorial Logic Gates.** Inspired by these observations, we have used the present system to construct combinatorial logic gates. First, the inputs used in “INHIBIT” logic gate presented in Figure 4C, *h*-TELO ( $K^+$ ) and DNase I, were integrated into another “INHIBIT” logic gate by adding a third input T7 Endonuclease I (T7 Endo I). The fluorescence response at 530 nm has been used as output. Since 4 equiv T7 Endo I can digest the Cz-stabilized *h*-TELO, it can modulate the logic function. The operational details of the logic system is shown in the Figure 7A–D and Figure S21 in the Supporting Information. The logic gate had an output of “1” (fluorescence turn-on), when the input was (1,0,0) (Figure S21, SI). However, the presence of other inputs demonstrated an output of “0” (fluorescence turn-off). This combination of logic gates could be realized as a process that the output of one INHIBIT logic gate was used as input of another INHIBIT logic gate. The successful implementation of this three-input INHIBIT–INHIBIT combinatorial gate may open up new avenues for other complex higher-order integrated circuits.

Next, a two-input two-output logic gate has also been constructed based on the Cz-stabilized *h*-TELO platform in the presence of DNase I and T7 Endo I as two inputs. The fluorescence responses at 530 and 373 nm have been used as two outputs. As shown in Figure 7E–H, the true output of “1” (fluorescence turn-on) at output<sub>530</sub> (530 nm) was observed only when the input was (0,0), while the other input states [(1,0), (0,1) and (1,1)] displayed a false output “0”

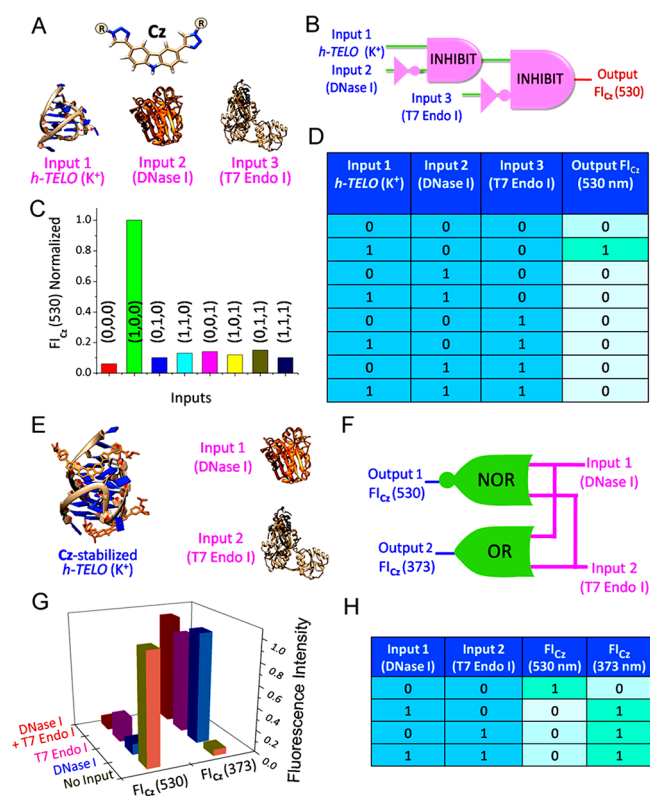


**Figure 7.** Combinatorial logic gates: (A) Schematic representation of the operation of INHIBIT–INHIBIT logic system; (B) Logic representation; (C) Normalized fluorescence response corresponding to each input; (D) The truth table of INHIBIT–INHIBIT logic system; (E) Schematic representation of the operation of NOR–OR logic system; (F) Logic representation; (G) Normalized fluorescence response corresponding to each input; (H) The truth table of NOR–OR logic system. For logic operation 1  $\mu$ M of Cz, *h*-TELO ( $K^+$ ), DNase I and 4  $\mu$ M of T7 Endo I were used. The details have been described in the Supporting Information.

(fluorescence turn-off) (Figure S22, SI). In contrast, the inputs of (1,0), (0,1) and (1,1) yields a true output “1” and displayed a false output “0” with input (0,0) at output<sub>373</sub> (373 nm). The truth table for this system is consistent with NOR gate at output<sub>530</sub> and OR gate at output<sub>373</sub>. This dual output NOR–OR system can be used in the development of demultiplexers.<sup>65</sup>

**Logic System for the Identification of Nonzero Square Numbers.** The Cz-stabilized *h*-TELO platform can be coupled with numerous nuclease enzymes to execute programmed function. Herein we demonstrate a proof of principle by identification of nonzero square numbers up to 16. We converted every whole number (up to 16) into a four-bit binary number by different combination of the inputs (nuclease S1, Exo I, T7 Endo I and DNase I) (Figure S23, SI). The fluorescence response at 530 nm has been used as output. The detailed description and results of the four-input binary logic operation are shown in Figures S23–S25 in the Supporting Information. The square numbers (1, 4, 9, 16) demonstrated an output of “1” (fluorescence turn-on), whereas an output of “0” was observed for the rest of the numbers. Therefore, it could be assumed that this system can be modulated to carry out complex calculations by varying inputs.

## CONCLUSION

In conclusion, we have used a microenvironment sensitive probe Cz that simultaneously detects *h*-TELO and nucleases with distinct fluorescence turn-on responses. The probe Cz selectively binds and stabilizes *h*-TELO G-quadruplex over other quadruplexes and duplex DNA. The differential fluorescence behavior of Cz-stabilized *h*-TELO in the presence of nucleases has been used to develop a sensor device to detect the activity of DNase I. The enzymatic activity of nuclease S1 or DNase I on Cz-stabilized *h*-TELO structure has been used to construct YES and INHIBIT logic systems. By using DNase I and *h*-TELO as inputs, a logic system with multireset function is established that can be recycled for three cycles. In addition, combinatorial INHIBIT–INHIBIT and NOR–OR logic systems have been demonstrated. Furthermore, a complex logic system has been constructed for the identification of nonzero square numbers up to 16. Taken together, the development of DNA based logic device modulated by small molecules and enzymes may be useful for designing intelligent biomolecular machines.

Since the enzymatic reactions described here are very sensitive, the application of the enzyme regulated logic systems in diverse operating conditions such as temperature, pH, time *etc.* is a challenging task. A number of external effectors may influence the outcome of logic systems. As a result, practical applications of enzyme regulated logic systems are challenging. The present study reports a promising strategy to construct DNA based nanodevices that may open up new avenues for the development of complex logic systems by utilizing a range of DNA interacting small molecules, nucleases and their specific interactions with different nucleic acid structures.

## MATERIALS AND METHODS

**General Materials.** The general chemicals and labeled DNA sequences required for biophysical analysis were purchased from Sigma-Aldrich. The DNA sequences of highest purity were purchased for best results. The nuclease S1 from *Aspergillus oryzae* was purchased from Sigma-Aldrich. The DNase I from *Bovine pancreas* was purchased from Sigma-Aldrich. Exonuclease I and III were purchased from Thermo Fisher Scientific. T7 Endonuclease I was purchased from NEB, England.

**Fluorescence Binding Titration with DNA Targets.** The fluorescence experiments were carried out using a Horiba Jobin Yvon Fluorolog-3 instrument at 25 °C in a thermostated cell holder using quartz cuvette of 1 mm path-length. For fluorescence titration of Cz with G-quadruplexes, 200  $\mu$ M *c*-MYC, *c*-KIT1, *c*-KIT2 and a self-complementary hairpin *ds* DNA were preannealed in filtered and degassed 10 mM Tris-HCl, 100 mM KCl buffer (pH 7.4) by heating at 95 °C and subsequent cooling to room temperature. Similarly, the 24-mer polymorphic *h*-TELO sequence was annealed in 10 mM Tris-HCl, 100 mM KCl buffer (pH 7.4) to adopt a mixed hybrid conformation, *i.e.*, *h*-TELO ( $K^+$ ). The *h*-TELO sequence was annealed in 10 mM Tris-HCl, 100 mM NaCl buffer (pH 7.4) to form antiparallel G-quadruplex structure, *h*-TELO ( $Na^+$ ). The *h*-TELO sequence was also annealed in Milli-Q (MQ) water (pH 7.4) in the absence of salt, *i.e.*, *h*-TELO (free).

To a solution of Cz (1  $\mu$ M), the preannealed DNA quadruplexes were added in a stepwise manner (0–4 equiv) and subsequently the fluorescence emission was recorded after a 2 min equilibration period. Cz was excited at 320 nm and the

fluorescence emission spectra were recorded from 335 to 560 nm using 4 nm bandpass filters. The spectral data represents the mean of three scans and the final analysis of the data was carried out using OriginPro 8.0.

Sequences used in this study were as follows:

*h-TELO*: 5'-d(T<sub>2</sub>G<sub>3</sub>T<sub>2</sub>AG<sub>3</sub>T<sub>2</sub>AG<sub>3</sub>T<sub>2</sub>AG<sub>3</sub>A)-3'.

*c-MYC*: 5'-d(TGAG<sub>3</sub>TG<sub>3</sub>TAG<sub>3</sub>TG<sub>3</sub>TA<sub>2</sub>)-3'.

*c-KIT1*: 5'-d(G<sub>3</sub>AG<sub>3</sub>CGCTG<sub>3</sub>AG<sub>3</sub>AG<sub>3</sub>)-3'.

*c-KIT2*: 5'-d(G<sub>3</sub>CG<sub>3</sub>CGCGAG<sub>3</sub>AG<sub>4</sub>)-3'.

*ds* DNA: 5'-d(TATAGCTATA HEG TATAGCTAT A)-3'.

HEG = Hexaethylene glycol.

The recorded spectral data was used to determine the dissociation constant of the ligands for quadruplexes using the Hill-1 eq 1:

$$F = F_0 + \frac{(F_{\max} - F_0)[\text{DNA}]}{K_d + [\text{DNA}]} \quad (1)$$

$F$  is the fluorescence intensity,  $F_{\max}$  is the maximum fluorescence intensity,  $F_0$  is the fluorescence intensity in the absence of DNA and  $K_d$  is the dissociation constant.

**FRET Melting Analysis.** Stock solution of *Cz* (200  $\mu\text{M}$ ) was prepared in MQ water (pH 7.4). Dual labeled parallel-type oncogenic promoter G-quadruplex forming sequences (*c-MYC*, *c-KIT1* and *c-KIT2*) and a self-complementary hairpin duplex (*ds*) DNA sequence were diluted in 50 mM potassium cacodylate buffer (pH 7.4) and annealed at a concentration of 200 nM by heating at 95 °C for 5 min followed by cooling to room temperature. The dual labeled *h-TELO* sequence was similarly diluted and annealed in 50 mM sodium cacodylate buffer (pH 7.4), 50 mM potassium cacodylate buffer (pH 7.4) and MQ water (pH 7.4) to give antiparallel quadruplex, mixed hybrid-type quadruplex and free *h-TELO* (in the absence of salt), respectively. The 96-well plates were prepared by aliquoting 50  $\mu\text{L}$  of the annealed DNA into each well, followed by 50  $\mu\text{L}$  of *Cz* at different concentrations (0.05, 0.1, 0.2, 0.5, 1.0  $\mu\text{M}$ ). Measurements were made in triplicate with an excitation wavelength of 483 nm and a detection wavelength of 533 nm using a LightCycler 480-II System RT-PCR machine (Roche). Final analysis of the data was carried out using OriginPro 8.0 data analysis.

Sequences used in this study were as follows:

*h-TELO*: 5'-FAM-d(T<sub>2</sub>G<sub>3</sub>T<sub>2</sub>AG<sub>3</sub>T<sub>2</sub>AG<sub>3</sub>T<sub>2</sub>AG<sub>3</sub>A)-TAMRA-3'.

*c-MYC*: 5'-FAM-d(TGAG<sub>3</sub>TG<sub>3</sub>TAG<sub>3</sub>TG<sub>3</sub>TA<sub>2</sub>)-TAMRA-3'.

*c-KIT1*: 5'-FAM-d(G<sub>3</sub>AG<sub>3</sub>CGCTG<sub>3</sub>AG<sub>3</sub>AG<sub>3</sub>)-TAMRA-3'.

*c-KIT2*: 5'-FAM-d(G<sub>3</sub>CG<sub>3</sub>CGCGAG<sub>3</sub>AG<sub>4</sub>)-TAMRA-3'.

*ds* DNA: 5'-FAM-d(TATAGCTATA HEG TATAGCTA-TA)-TAMRA-3'.

**CD Spectroscopy.** CD spectra were recorded on a JASCO J-815 spectrophotometer by using a 1 mm path length quartz cuvette. Aliquots of *Cz* were added stepwise to 5  $\mu\text{M}$  preannealed *h-TELO* quadruplex sequence (5'-d(T<sub>2</sub>G<sub>3</sub>T<sub>2</sub>AG<sub>3</sub>T<sub>2</sub>AG<sub>3</sub>T<sub>2</sub>AG<sub>3</sub>A)-3') in degassed MQ water (pH 7.4), 10 mM Tris-HCl, 100 mM NaCl buffer (pH 7.4) and 10 mM Tris-HCl, 100 mM KCl buffer (pH 7.4), respectively. The CD spectra were recorded upon incremental addition of *Cz* to the *h-TELO* between 200 to 500 nm. For nucleases, CD spectra were recorded upon incremental addition of *Cz* (0–4 equiv) to the 10  $\mu\text{M}$  of nuclease S1 and DNase I. The CD spectra represent an average of three scans and were smoothed and zero corrected. Final analysis of the data was carried out by using OriginPro 8.0.

**Fluorescence Binding Titration with Nucleases.** For fluorescence titration of *Cz* with nuclease S1 and DNase I, nucleases (10 mg) were dissolved in the respective buffers to make stock solutions of 294  $\mu\text{M}$  nuclease S1 (50% glycerol, 20 mM Tris-HCl (pH 7.4), 30 mM KCl, 0.5 mM EDTA, 1 mM DTT buffer) and 322  $\mu\text{M}$  DNase I (10 mM Tris-HCl (pH 7.4), 2.5 mM MgCl<sub>2</sub>, 0.1 mM CaCl<sub>2</sub>). Fluorescence spectra were recorded upon stepwise addition of nucleases (0–2  $\mu\text{M}$ ) to *Cz* (1  $\mu\text{M}$ ) using a Horiba Jobin Yvon Fluorolog-3 instrument at 25 °C in a thermostated cell holder using quartz cuvette of 1 mm path-length. *Cz* was excited at 320 nm and the fluorescence emission spectra were monitored from 335 to 560 nm using 4 nm bandpass filters. Binding dissociation constant ( $K_d$ ) was calculated using the Hill-1 eq 1. The spectral data represents the mean of three scans and the final analysis of the data was carried out using OriginPro 8.0.

A reverse titration of the nucleases (nuclease S1 and DNase I) with *Cz* was carried out. Fluorescence spectra were recorded upon incremental addition of *Cz* (0–4  $\mu\text{M}$ ) to nuclease S1 (2  $\mu\text{M}$ ) and DNase I (2  $\mu\text{M}$ ) in respective buffers. The nucleases were excited at 280 nm and the fluorescence emission spectra were monitored from 300 to 500 nm using 4 nm bandpass filters using a Horiba JobinYvon Fluorolog 3 instrument at 25 °C in a thermostated cell holder using quartz cuvette of 1 mm path-length.

**Fluorescence Titration of *Cz* in Different Solvent Environments.** Fluorescence spectra was recorded after diluting *Cz* in different solvents (hexane, acetone, ethyl acetate, DCM, ethanol, methanol, water *etc.*) to a final concentration of 1  $\mu\text{M}$ . *Cz* was excited at 320 nm and the fluorescence emission spectra were monitored from 335 to 560 nm using 4 nm bandpass filters.

**Fluorescence Binding Assay to Monitor the Activity of Nucleases.** To evaluate the activity of the nucleases, 500  $\mu\text{M}$  *h-TELO* ( $K^+$ ) was prepared by heat annealing *h-TELO* sequence in 10 mM Tris-HCl, 100 mM KCl buffer (pH 7.4). A mixture of (1:1) *h-TELO* ( $K^+$ ) (1  $\mu\text{M}$ ) and nucleases (nuclease S1 and DNase I) was prepared in nuclease S1 and DNase I buffers. *Cz* (1  $\mu\text{M}$ ) was titrated with 0–1 equiv of this mixture and the fluorescence spectra were recorded from 335 to 560 nm ( $\lambda_{\max}^{\text{em}} = 320$  nm) after each addition.

To investigate the ability of *Cz* to protect *h-TELO* against nuclease digestion, *Cz* (1  $\mu\text{M}$ ) (50% glycerol, 20 mM Tris-HCl (pH 7.4), 30 mM KCl, 0.5 mM EDTA, 1 mM DTT buffer) was added to preannealed free *h-TELO* (2  $\mu\text{M}$ ) or *h-TELO* ( $K^+$ ) (1  $\mu\text{M}$ ) and the fluorescence emission was recorded after a 2 min equilibration period. Then nuclease S1 was added to the mixture in a stepwise manner (0–1 equiv of DNA) and fluorescence spectra were recorded after each addition and subsequent incubation of the mixture in 37 °C water bath for 5 min.

For DNase I, preannealed free *h-TELO* (2  $\mu\text{M}$ ) and 1  $\mu\text{M}$  *h-TELO* ( $K^+$ ) were added to *Cz* (1  $\mu\text{M}$ ) in 10 mM Tris-HCl (pH 7.4), 2.5 mM MgCl<sub>2</sub>, 0.1 mM CaCl<sub>2</sub> buffer. Then fluorescence spectra were recorded after incremental addition (0–1 equiv of DNA) of DNase I and subsequent incubation of the mixture in water bath (37 °C) for 5 min. Similarly, preannealed 1  $\mu\text{M}$  *h-TELO* ( $K^+$ ) and *Cz* (1  $\mu\text{M}$ ) were mixed and fluorescence spectra were recorded after titrating with (0–4  $\mu\text{M}$ ) Exo I, Exo III and T7 endonuclease I. Final analysis of the data was carried out using OriginPro 8.0.

The nuclease sensor calibration curve,  $F/F_0$  was plotted as sensor signal, where  $F_0$  is the fluorescence intensity of the

sensor solution in the absence of nucleases;  $F$  is the fluorescence intensity of the sensor solution upon addition of different concentrations of nucleases. As for the nuclease detection assay,  $F/F_0$  was plotted as sensor signal with increasing nuclease concentration (0–2  $\mu\text{M}$ ). All the measurements were performed three times, and the standard deviation was plotted as the error bar.

**Reusable Logic Device with Multireset Function.** For recycling experiments,  $Cz$  was taken in 10 mM Tris-HCl, 100 mM KCl, 2.5 mM  $\text{MgCl}_2$ , 0.1 mM  $\text{CaCl}_2$  buffer (pH 7.4) at the final concentration of 1  $\mu\text{M}$ . First, 1  $\mu\text{M}$   $h\text{-TELO}$  ( $\text{K}^+$ ) was added to  $Cz$  (1  $\mu\text{M}$ ) and the corresponding fluorescence spectra were recorded from 335 to 560 nm ( $\lambda_{\text{max}}^{\text{em}} = 320$  nm) after 2 min equilibration. Next, the digestion of  $h\text{-TELO}$  ( $\text{K}^+$ ) was carried out by adding 1 equiv of DNase I (with respect to DNA) to the mixture and incubating the mixture in a 37 °C water bath for 15 min. After digestion, the fluorescence emission spectra were again recorded. The DNase I was then deactivated by heating the mixture at 80 °C in dry bath for 15 min and then allowed to cool to room temperature. In the second cycle, again  $h\text{-TELO}$  ( $\text{K}^+$ ) and DNase I were added and after each addition, emission spectra were recorded. The third cycle was again started with heat deactivation of the mixture as described above. A total of three cycles was performed in Horiba Jobin Yvon FluoroLog-3 instrument and the spectral data was analyzed using OriginPro 8.0.

## ■ ASSOCIATED CONTENT

### ● Supporting Information

The Supporting Information is available free of charge on the ACS Publications website at DOI: 10.1021/acssynbio.8b00088.

Fluorescence, CD data, truth tables (PDF)

## ■ AUTHOR INFORMATION

### Corresponding Author

\*E-mail: ocjd@iacs.res.in.

### ORCID

Jyotirmayee Dash: 0000-0003-4130-2841

### Notes

The authors declare no competing financial interest.

## ■ ACKNOWLEDGMENTS

This work was supported by the Department of Science and Technology [DST/ SJF/CSA-01/2015–16] and the Department of Biotechnology [6242-P31/RGCB/PMD/DBT/JTDH/2015], India. JD thanks DST for a SwarnaJayanti fellowship. MD and RP thank DST, India for INSPIRE fellowships.

## ■ REFERENCES

- (1) Linn, S. M., Lloyd, R. S., and Roberts, R. J. (1993) Preface/Front Matter, In *Nucleases*, 2nd ed., Cold Spring Harbor Laboratory Press, Cold Spring Harbor, NY.
- (2) Munoz, P., Blanco, R., Flores, J. M., and Blasco, M. A. (2005) XPF nuclease-dependent telomere loss and increased DNA damage in mice overexpressing TRF2 result in premature aging and cancer. *Nat. Genet.* 37, 1063–1071.
- (3) Singh, P., Yang, M., Dai, H., Yu, D., Huang, Q., Tan, W., Kernstine, K., Lin, D., and Shen, B. (2008) Over-expression and hypomethylation of flap endonuclease 1 gene in breast and other cancers. *Mol. Cancer Res.* 6, 1710–1717.

- (4) Hernandez, L. I., Ozalp, V. C., and Hernandez, F. J. (2016) Nuclease activity as a specific biomarker for breast cancer. *Chem. Commun.* 52, 12346–12349.

- (5) Riehemann, K., Schneider, S. W., Luger, T. A., Godin, B., Ferrari, M., and Fuchs, H. (2009) Nanomedicine—challenge and perspectives. *Angew. Chem., Int. Ed.* 48, 872–897.

- (6) Feng, X., Duan, X., Liu, L., Feng, F., Wang, S., Li, Y., and Zhu, D. (2009) Fluorescence Logic-Signal-Based Multiplex Detection of Nucleases with the Assembly of a Cationic Conjugated Polymer and Branched DNA. *Angew. Chem., Int. Ed.* 48, 5316–5321.

- (7) Guo, Y., Xu, L., Hong, S., Sun, Q., Yao, W., and Pei, R. (2016) Label-free DNA-based biosensors using structure-selective light-up dyes. *Analyst* 141, 6481–6489.

- (8) Lu, L., Shiu-Hin Chan, D., Kwong, D. W. J., He, H.-Z., Leung, C.-H., and Ma, D.-L. (2014) Detection of nicking endonuclease activity using a G-quadruplex-selective luminescent switch-on probe. *Chem. Sci.* 5, 4561–4568.

- (9) Lee, J., Kim, Y.-K., and Min, D.-H. (2011) A New Assay for Endonuclease/Methyltransferase Activities Based on Graphene Oxide. *Anal. Chem.* 83, 8906–8912.

- (10) O'Steen, M. R., Cornett, E. M., and Kolpashchikov, D. M. (2015) Nuclease-containing media for resettable operation of DNA logic gates. *Chem. Commun.* 51, 1429–1431.

- (11) Zhang, X., Cheng, R., Shi, Z., and Jin, Y. (2017) Label-free detection of EcoRI endonuclease activity via fluorescent DNA logic gate. *Sens. Actuators, B* 244, 387–392.

- (12) de Silva, P. A., Gunaratne, N. H. Q., and McCoy, C. P. (1993) A molecular photoionic AND gate based on fluorescent signalling. *Nature* 364, 42–44.

- (13) Okamoto, A., Tanaka, K., and Saito, I. (2004) DNA Logic Gates. *J. Am. Chem. Soc.* 126, 9458–9463.

- (14) Frezza, B. M., Cockroft, S. L., and Ghadiri, M. R. (2007) Modular Multi-Level Circuits from Immobilized DNA-Based Logic Gates. *J. Am. Chem. Soc.* 129, 14875–14879.

- (15) Famulok, M., Hartig, J. S., and Mayer, G. (2007) Functional Aptamers and Aptazymes in Biotechnology. *Chem. Rev.* 107, 3715–3743.

- (16) de Silva, A. P., and Uchiyama, S. (2007) Molecular logic and computing. *Nat. Nanotechnol.* 2, 399–410.

- (17) Margulies, D., and Hamilton, A. D. (2009) Digital Analysis of Protein Properties by an Ensemble of DNA Quadruplexes. *J. Am. Chem. Soc.* 131, 9142–9143.

- (18) Li, T., Dong, S., and Wang, E. A. (2010) Lead(II)-Driven DNA Molecular Device for Turn-On Fluorescence Detection of Lead(II) Ion with High Selectivity and Sensitivity. *J. Am. Chem. Soc.* 132, 13156–13157.

- (19) Katz, E., and Privman, V. (2010) Enzyme-based logic systems for information processing. *Chem. Soc. Rev.* 39, 1835–1857.

- (20) Genot, A. J., Bath, J., and Turberfield, A. J. (2011) Reversible Logic Circuits Made of DNA. *J. Am. Chem. Soc.* 133, 20080–20083.

- (21) Prokup, A., Hemphill, J., and Deiters, A. (2012) DNA Computation: A Photochemically Controlled AND Gate. *J. Am. Chem. Soc.* 134, 3810–3815.

- (22) Zhou, Z., Zhu, J., Zhang, L., Du, Y., Dong, S., and Wang, E. (2013) G-quadruplex-Based Fluorescent Assay of S1 Nuclease Activity and  $\text{K}^+$ . *Anal. Chem.* 85, 2431–2435.

- (23) Fernandez-Rodriguez, J., Yang, L., Gorochowski, T. E., Gordon, D. B., and Voigt, C. A. (2015) Memory and Combinatorial Logic Based on DNA Inversions: Dynamics and Evolutionary Stability. *ACS Synth. Biol.* 4, 1361–1372.

- (24) Miyamoto, T., Razavi, S., DeRose, R., and Inoue, T. (2013) Synthesizing Biomolecule-Based Boolean Logic Gates. *ACS Synth. Biol.* 2, 72–82.

- (25) You, M., Zhu, G., Chen, T., Donovan, M. J., and Tan, W. (2015) Programmable and Multiparameter DNA-Based Logic Platform For Cancer Recognition and Targeted Therapy. *J. Am. Chem. Soc.* 137, 667–674.

- (26) Varghese, S., Elemans, J. A. A. W., Rowan, A. E., and Nolte, R. J. M. (2015) Molecular computing: paths to chemical Turing machines. *Chem. Sci.* 6, 6050–6058.
- (27) Andreasson, J., and Pischel, U. (2015) Molecules with a sense of logic: a progress report. *Chem. Soc. Rev.* 44, 1053–1069.
- (28) Elbaz, J., Moshe, M., and Willner, I. (2009) Coherent Activation of DNA Tweezers: A “SET–RESET” Logic System. *Angew. Chem., Int. Ed.* 48, 3834–3837.
- (29) Mendoza, O., Mergny, J.-L., Aimé, J.-P., and Elezgaray, J. (2016) G-Quadruplexes Light up Localized DNA Circuits. *Nano Lett.* 16, 624–628.
- (30) Privman, V. (2010) Biomolecular computing: Learning through play. *Nat. Nanotechnol.* 5, 767–768.
- (31) Orbach, R., Willner, B., and Willner, I. (2015) Catalytic nucleic acids (DNAzymes) as functional units for logic gates and computing circuits: from basic principles to practical applications. *Chem. Commun.* 51, 4144–4160.
- (32) Zong, C., Ai, K., Zhang, G., Li, H., and Lu, L. (2011) Dual-Emission Fluorescent Silica Nanoparticle-Based Probe for Ultra-sensitive Detection of Cu<sup>2+</sup>. *Anal. Chem.* 83, 3126–3132.
- (33) Bowers, D. T., Tanes, M. L., Das, A., Lin, Y., Keane, N. A., Neal, R. A., Ogle, M. E., Brayman, K. L., Fraser, C. L., and Botchwey, E. A. (2014) Spatiotemporal Oxygen Sensing Using Dual Emissive Boron Dye–Polylactide Nanofibers. *ACS Nano* 8, 12080–12091.
- (34) Li, H., Peng, W., Feng, W., Wang, Y., Chen, G., Wang, S., Li, S., Li, H., Wang, K., and Zhang, J. (2016) A novel dual-emission fluorescent probe for the simultaneous detection of H<sub>2</sub>S and GSH. *Chem. Commun.* 52, 4628–4631.
- (35) Zhao, Y., Shi, C., Yang, X., Shen, B., Sun, Y., Chen, Y., Xu, X., Sun, H., Yu, K., Yang, B., and Lin, Q. (2016) pH- and Temperature-Sensitive Hydrogel Nanoparticles with Dual Photoluminescence for Bioprobes. *ACS Nano* 10, 5856–5863.
- (36) Fan, D., Zhu, J., Zhai, Q., Wang, E., and Dong, S. (2016) Cascade DNA logic device programmed ratiometric DNA analysis and logic devices based on a fluorescent dual-signal probe of a G-quadruplex DNAzyme. *Chem. Commun.* 52, 3766–3769.
- (37) Wiegand, R. C., Godson, G. N., and Radding, C. M. (1975) Specificity of the S1 nuclease from *Aspergillus oryzae*. *J. Biol. Chem.* 250, 8848–8855.
- (38) Davis, J. T. (2004) G-Quartets 40 Years Later: From 5′-GMP to Molecular Biology and Supramolecular Chemistry. *Angew. Chem., Int. Ed.* 43, 668–698.
- (39) Yang, P., De Cian, A., Teulade-Fichou, M.-P., Mergny, J.-L., and Monchaud, D. (2009) Engineering Bisquinolinium/Thiazole Orange Conjugates for Fluorescent Sensing of G-Quadruplex DNA. *Angew. Chem., Int. Ed.* 48, 2188–2191.
- (40) Balasubramanian, S., and Neidle, S. (2009) G-quadruplex nucleic acids as therapeutic targets. *Curr. Opin. Chem. Biol.* 13, 345–353.
- (41) Balasubramanian, S., Hurley, L. H., and Neidle, S. (2011) Targeting G-quadruplexes in gene promoters: a novel anticancer strategy? *Nat. Rev. Drug Discovery* 10, 261–275.
- (42) Neidle, S. (2016) Quadruplex Nucleic Acids as Novel Therapeutic Targets. *J. Med. Chem.* 59, 5987–6011.
- (43) Huppert, J. L. (2008) Four-stranded nucleic acids: structure, function and targeting of G-quadruplexes. *Chem. Soc. Rev.* 37, 1375–1384.
- (44) Biffi, G., Tannahill, D., McCafferty, J., and Balasubramanian, S. (2013) Quantitative visualization of DNA G-quadruplex structures in human cells. *Nat. Chem.* 5, 182–186.
- (45) Maji, B., Kumar, K., Kaulage, M., Muniyappa, K., and Bhattacharya, S. (2014) Design and Synthesis of New Benzimidazole–Carbazole Conjugates for the Stabilization of Human Telomeric DNA, Telomerase Inhibition, and Their Selective Action on Cancer Cells. *J. Med. Chem.* 57, 6973–6988.
- (46) Hansel-Hertsch, R., Di Antonio, M., and Balasubramanian, S. (2017) DNA G-quadruplexes in the human genome: detection, functions and therapeutic potential. *Nat. Rev. Mol. Cell Biol.* 18, 279–284.
- (47) Tseng, T.-Y., Wang, Z.-F., Chien, C.-H., and Chang, T.-C. (2013) In-cell optical imaging of exogenous G-quadruplex DNA by fluorogenic ligands. *Nucleic Acids Res.* 41, 10605–10618.
- (48) Li, T., Wang, E., and Dong, S. (2009) Potassium–Lead-Switched G-Quadruplexes: A New Class of DNA Logic Gates. *J. Am. Chem. Soc.* 131, 15082–15083.
- (49) Zhu, J., Zhang, L., Dong, S., and Wang, E. (2013) Four-Way Junction-Driven DNA Strand Displacement and Its Application in Building Majority Logic Circuit. *ACS Nano* 7, 10211–10217.
- (50) Bhowmik, S., Das, R. N., Parasar, B., and Dash, J. (2013) pH dependent multifunctional and multiply-configurable logic gate systems based on small molecule G-quadruplex DNA recognition. *Chem. Commun.* 49, 1817–1819.
- (51) Zhang, L., Zhu, J., Guo, S., Li, T., Li, J., and Wang, E. (2013) Photoinduced Electron Transfer of DNA/Ag Nanoclusters Modulated by G-Quadruplex/Hemin Complex for the Construction of Versatile Biosensors. *J. Am. Chem. Soc.* 135, 2403–2406.
- (52) Leung, C.-H., Zhong, H.-J., He, H.-Z., Lu, L., Chan, D.S.-H., and Ma, D.-L. (2013) Luminescent oligonucleotide-based detection of enzymes involved with DNA repair. *Chem. Sci.* 4, 3781–3795.
- (53) Ma, D.-L., He, H.-Z., Chan, D.S.-H., and Leung, C.-H. (2013) Simple DNA-based logic gates responding to biomolecules and metal ions. *Chem. Sci.* 4, 3366–3380.
- (54) Guo, Y., Zhou, L., Xu, L., Zhou, X., Hu, J., and Pei, R. (2015) Multiple types of logic gates based on a single G-quadruplex DNA strand. *Sci. Rep.* 4, 7315.
- (55) Fan, D., Wang, E., and Dong, S. (2017) A DNA-based parity generator/checker for error detection through data transmission with visual readout and an output-correction function. *Chem. Sci.* 8, 1888–1895.
- (56) Albada, H. B., Golub, E., and Willner, I. (2016) Rational design of supramolecular hemin/G-quadruplex-dopamine aptamer nucleozyme systems with superior catalytic performance. *Chem. Sci.* 7, 3092–3101.
- (57) He, H.-Z., Chan, D.S.-H., Leung, C.-H., and Ma, D.-L. (2013) G-quadruplexes for luminescent sensing and logic gates. *Nucleic Acids Res.* 41, 4345–4359.
- (58) Gao, R.-R., Shi, S., Zhu, Y., Huang, H.-L., and Yao, T.-M. (2016) A RET-supported logic gate combinatorial library to enable modeling and implementation of intelligent logic functions. *Chem. Sci.* 7, 1853–1861.
- (59) Debnath, M., Ghosh, S., Panda, D., Bessi, I., Schwalbe, H., Bhattacharyya, K., and Dash, J. (2016) Small molecule regulated dynamic structural changes of human G-quadruplexes. *Chem. Sci.* 7, 3279–3285.
- (60) Chang, C.-C., Wu, J.-Y., Chien, C.-W., Wu, W.-S., Liu, H., Kang, C.-C., Yu, L.-J., and Chang, T.-C. (2003) A Fluorescent Carbazole Derivative: High Sensitivity for Quadruplex DNA. *Anal. Chem.* 75, 6177–6183.
- (61) Renčič, D., Zhou, J., Beaurepaire, L., Guédin, A., Bourdoncle, A., and Mergny, J.-L. (2012) A FRET-based screening assay for nucleic acid ligands. *Methods* 57, 122–128.
- (62) Gao, Y., He, T., Hu, P., Koh, T. M., Sun, H., and Grimsdale, A. C. (2014) Influence of H-Bonding on Self-Assembly and Tunable Dual-Emission of Carbazole-Based Zn(II)-Terpyridine Metallocomplexes. *Macromol. Chem. Phys.* 215, 753–762.
- (63) Bayda, M., Angulo, G., Hug, G. L., Ludwiczak, M., Karolczak, J., Koput, J., Dobkowski, J., and Marciniak, B. (2017) Electron transfer in silicon-bridged adjacent chromophores: the source for blue-green emission. *Phys. Chem. Chem. Phys.* 19, 11404–11415.
- (64) Imai, Y., Kawai, T., and Yuasa, J. (2016) OFF–ON–OFF Dual Emission at Visible and UV Wavelengths from Carbazole Functionalized  $\beta$ -Diketone Europium(III) Complex. *J. Phys. Chem. A* 120, 4131–4138.
- (65) Gao, R.-R., Yao, T.-M., Lv, X.-Y., Zhu, Y.-Y., Zhang, Y.-W., and Shi, S. (2017) Integration of G-quadruplex and DNA-templated Ag NCs for nonarithmetic information processing. *Chem. Sci.* 8, 4211–4222.